Journal of Carbon Research

MDPI

Article

Fabrication of Carbon Nanotubes Derived from Waste Tire Pyrolytic Carbon and Their Application in the Dehydrogenation of Methylcyclohexane to Produce Hydrogen

Hongli Ye [1,2,3], Shuangxi Liu [3,4], Dongmei Huang [1], Chaojun Jiang [1], Rui Yuan [1] and Cui Zhang [3,4,*]

[1] Laboratory of Aquatic Product Quality and Safety and Processing, Key Laboratory of Oceanic and Polar Fisheries, Ministry of Agriculture and Rural Affairs, East China Sea Fisheries Research Institute, Chinese Academy of Fishery Sciences, Shanghai 200090, China; yehongli@ecsf.ac.cn (H.Y.); huangdm@ecsf.ac.cn (D.H.); beileijh@163.com (C.J.); yuanrui@ecsf.ac.cn (R.Y.)
[2] Key Laboratory of Control of Safety and Quality for Aquatic Product, Ministry of Agriculture and Rural Affairs, Beijing 100141, China
[3] Institute of New Catalytic Materials Science and MOE Key Laboratory of Advanced Energy Materials Chemistry, School of Materials Science and Engineering, National Institute of Advanced Materials, Nankai University, Tianjin 300350, China; sxliu@nankai.edu.cn
[4] Collaborative Innovation Center of Chemical Science and Engineering (Tianjin), Tianjin 300072, China
* Correspondence: zhangcui@nankai.edu.cn

Abstract: The accumulation of waste tires has resulted in very urgent environmental problems. Pyrolysis has been regarded as a green eco-friendly technology to deal with waste tires, and it is vital to make use of the pyrolysis carbon. Herein, we propose a new way to utilize pyrolysis carbon, to prepare carbon nanotubes with the help of ferrocene. The optimal preparation processes were determined by optimizing the parameters including the solvent, temperature, time, etc. The results of scanning electron microscopy and transmission electron microscopy evidenced the successful formation of carbon nanotubes. Meanwhile, the Brunauer–Emmett–Teller (BET) method and N_2-adsorption showed that the yielded carbon nanotubes featured a large surface area and abundant pore structure in comparison with the pyrolytic carbon. Finally, the as-prepared carbon nanotubes were applied as the supports for Pt-based catalysts for the dehydrogenation of methylcyclohexane to produce hydrogen. The results showed that the Pt/carbon-nanotubes catalyst exhibited the highest conversion of methylcyclohexane (28.6%), stability, and hydrogen evolution rate (336.9 mmol/g_{Pt}/min) compared to the resulting Pt/commercial-activated-carbon (13.6% and 160.2 mmol/g_{Pt}/min) and Pt/pyrolytic-carbon catalysts (0.19% and 2.23 mmol/g_{Pt}/min).

Keywords: waste tires; pyrolytic carbon; carbon nanotubes; dehydrogenation; methylcyclohexane

Citation: Ye, H.; Liu, S.; Huang, D.; Jiang, C.; Yuan, R.; Zhang, C. Fabrication of Carbon Nanotubes Derived from Waste Tire Pyrolytic Carbon and Their Application in the Dehydrogenation of Methylcyclohexane to Produce Hydrogen. *C* **2023**, *9*, 121. https://doi.org/10.3390/c9040121

Academic Editors: Sergey Mikhalovsky and Jinliang Song

Received: 28 September 2023
Revised: 8 December 2023
Accepted: 14 December 2023
Published: 16 December 2023

1. Introduction

As people's living standards improve and the automobile industry develops, the annual accumulation of discarded tires has become a very serious threat to the environment due to their non-biodegradability [1–3]. The amount of waste tires reached 200 million tons by 2020 and has further increased by 6 to 8% per year in China [4]. This increasingly serious problem requires the technological use of abandoned tires. Compared to direct landfill and incineration, pyrolysis of the discarded tires has been considered the most promising and efficient method to solve the problem due to the advantages of pursuing the reduction in quantity, the high-value utilization of the recycled products, and especially the friendliness to the environment [5,6]. During the pyrolysis process, the waste tire rubber is decomposed into fuel gas, pyrolysis oil, and carbon black under the absence of oxygen or hypoxia, and the fuel gas can be burned to supplement the heat required for the pyrolysis process; meanwhile, the pyrolytic oil and carbon black can be used as fuel oil and commercial carbon black, respectively, after simple purification treatment [7].

As one of the main pyrolysis products, the utilization of pyrolysis carbon black plays a significant role in dealing with the waste tires. A number of researchers have focused on and discussed the formation of activated carbon derived from pyrolysis carbon black due to the similar composition and structure to industrial carbon black [8,9], which has been successfully applied in adsorption [10,11], electrochemical [12,13], catalysis [14–16], and other fields [17]. However, few studies have reported the production of carbon nanotubes (CNTs) originating from pyrolysis carbon black.

Liquid organic hydrides (boiling points: 80–200 °C) have emerged as a promising hydrogen carrier owing to their easy achievement of hydrogenation and dehydrogenation, large hydrogen storage capacity (6–8%), high security during transportation, etc. [18–21] Methylcyclohexane (MCH) has been proposed as a potential and satisfactory candidate for liquid organic hydrides for its high reversibility and the low toxicity of the dehydrogenation product [22,23], which accelerates the dehydrogenation reaction process in the presence of Pt-based catalysts over appropriate supports [24]. It is vital for the supports to improve the activity and stability of the Pt-based catalyst [25–30], and carbon materials have been widely applied to promote the dispersion of Pt atoms, due to their large surface area and abundant oxygen-containing groups [31], including activated carbons [32], carbon filters [33], carbon nanotubes [34], and so on. Kong et al. considered that the features of CNTs rendered them a promising catalyst support, with their excellent thermal/electrical conductivity, high specific surface areas, and favorable adsorption of hydrogen. Wang et al. [35] reported that 0.25% Pt/CNTs exhibited consistent catalytic activity to 1% Pt/Al_2O_3. However, there was less reported on CNTs prepared from pyrolysis carbon black derived from waste tires and applied as the dehydrogenation support for MCH for producing hydrogen, which provides a new path to deal with waste tires in an eco-friendly manner.

Herein, we propose a new way to deal with the waste tire pyrolysis carbon, and we developed the preparation of CNTs by pyrolysis carbon black derived from waste tires. The synthesized parameters of the solvent, temperature, and reaction time were investigated to yield the excellent performance of CNTs. The characterization of scanning electron microscopy (SEM) and transmission electron microscopy (TEM), X-ray diffraction (XRD), N_2-adsorption, Raman spectra, Fourier-transform infrared spectroscopy (FTIR), and X-ray photoelectron spectroscopy (XPS) were utilized to reveal that the as-prepared CNTs had the distinct tubular structure, large surface area, abundant pore structure, high graphitization degree, and major oxygen-containing functional groups in compassion of pyrolysis carbon black. Finally, the satisfactory CNTs were used as the support for Pt-based catalysts and successfully applied to catalyze the dehydrogenation of methylcyclohexane to produce hydrogen.

2. Materials and Methods

2.1. Chemicals and Reagents

Pyrolytic carbon derived from waste tires was purchased from Shanghai Greenman ECO Science and Technology Co., Ltd. (Shanghai, China). Chloroplatinic acid solution and ferrocene were purchased from Tianjin Jinhai Type Science and Technology Development Co., Ltd. (Tianjin, China), and Tianjin Xiensi Biochemical Technology Co., Ltd. (Tianjin, China), respectively. Toluene, MCH, dimethylsulfoxide (DMSO), and ethylene glycol were from Tianjin Jiangtian Chemical Technology Co., Ltd. (Tianjin, China). The commercial activated carbon (AC) was provided by Fujian Xin Charcoal Industry Co., Ltd. (Shaowu, China). Milli-Q water (Millipore, 18.2 $M\Omega \cdot cm^{-1}$) was utilized throughout the experiments.

2.2. Instrumentations

SEM and TEM images were performed on a JEOL JSM-7500F (JEOL, Tokyo, Japan) and a FEI Tecnai G2 F20 (FEI, Eindhoven, The Netherlands), respectively. A microspores instrument ASAP 2020 (Micromeritics, Atlanta, GA, USA) and a Bruker D8 FOCUS diffractometer (Bruker, Karlsruhe, Germany) were used to analyze the pore structure and XRD patterns of the materials. The FTIR spectra and XPS profiles were measured by a Vector

22 Fourier-transform infrared spectrophotometer (Bruker, Fällanden, Switzerland) and a Kratos AXIS-ULTRA DLD multifunctional photoelectron spectrometer (Shimadzu, Kyoto, Japan), respectively. All the XPS peaks were calibrated with the C1s peak binding energy of 284.5 eV. The inductively coupled plasma atomic emission spectrometry (ICP-AES, ICP-9000 (N + M), Shimadzu, Kyoto, Japan) was utilized to calculate the load capacity of Pt. The TG and DTG curves were measure by a Thermo Plus EVO thermogravimetric differential thermal analyzer (TG-DTA, Rigaku, Tokyo, Japan) at a heating rate of 10 °C/min under nitrogen gas. All measurements were taken at room temperature.

2.3. Preparation of CNTs

The pyrolysis carbon derived from waste tires was extracted in toluene to remove the organic impurities and washed in dilute sulfuric acid to eliminate the inorganic ash (e.g., ZnS), which was marked as C. CNTs were synthesized by using the purified C as the carbon source and ferrocene as the catalyst with a mass ratio of 1:10 in dimethylsulfoxide solvent in a muffle furnace at 700~850 °C for 4~10 h.

2.4. Preparation of Pt/CNTs Catalyst

The Pt/CNTs catalyst was prepared as follows. First, 2.0 g of CNTs were uniformly dispersed into 20 mL of deionized water, and then a certain volume of chloroplatinic acid solution was slowly dropped into the suspension with a final Pt load amount of 0.2% and continuously stirred. After 30 min, 20 mL of ethylene glycol solution was sequentially added into the reaction system. The precursor reacted for 4 h, and the solid products (i.e., Pt/CNTs) were filtered, washed, and dried in a vacuum oven for 12 h at 55 °C. Meanwhile, C was used to synthesize the Pt/C catalyst as a contrast using the same operation. The Pt/CNTs and Pt/C catalysts were reduced by H_2 at 400 °C for 2 h and further applied to catalyze the dehydrogenation reaction of MCH.

2.5. The Dispersion of the Active Component Pt

The CO pulse technique was used to test the dispersion of the active component Pt. About 0.100 g of carbon materials was reduced by H_2 at 400 °C for 40 min, cooled to 25 °C under helium protection; then, the adsorption capacity of CO was tested.

2.6. Catalytic Reaction

The dehydrogenation reaction of methylcyclohexane to produce hydrogen was performed in a fixed-bed flow reactor (10 mm inner diameter (ID) × 250 mm) with the Pt-based catalyst weight of 0.30 g and the MCH flow rate of 0.03 mL/min. A Rock GC 7800 gas chromatograph and an SE-30 column were used to determine the conversion of MCH.

3. Results

3.1. Preparation and Characterizations of CNTs

The main chemical components of waste tire pyrolysis carbon black were carbon, oxygen, copper, zinc, etc., and its ash and fine powder content were relatively high, which could cause carbon deposition and lead to catalyst deactivation. Hence, it was significant to remove the ash before preparing carbon nanotubes. Meanwhile, pickling could not only effectively remove the ash on the surface of the pyrolytic carbon black but also increase the specific surface area and surface functional groups [16]. The preparation parameters were investigated to obtain the excellent properties, including the solvent, synthetic temperature, time, etc. In the SEM photos, the products without any solvent (Figure 1A) and those with the solvent of ultrapure water (Figures 1B and S1) were composed of angular and different size blocks, and a large number of amorphous spherical particles with a uniform size appeared; yet, no CNTs were observed. However, as displayed in Figure 1C, a large number of CNTs were discovered with the addition of DMSO, which might mean that the presence of DMSO was conducive to the sufficient and effective dispersal of the reactant, and CNTs were formed under the catalytic action of ferrocene. Meanwhile, as shown in

Figure 2, a small number of CNTs were formed at 700 °C, which was consistent with the report [36], the number continuously grew with the temperature increase to 750 °C and 800 °C, producing more energy and accelerating the catalytic reaction. However, some of the small carbon particles disappeared and became larger ones, which could possibly influence the surface area and pore structure; this was possibly caused by the excessive temperature. As depicted in Figure 3, the production and shape of CNTs at 6 h were better (such as in yield, length, shape, etc.) than those of CNTs at the other times with the field of view of 1 μm or 100 nm. Therefore, the CNTs were prepared at 750 °C or 800 °C for 6 h in DMSO in this work. TEM was utilized to study the morphology of the as-prepared CNTs. As displayed in Figure 4, the structures of the tube walls and inner cavity were clear and complete. The thickness of the tube wall was in the range of 2~8 nm; moreover, the internal diameter and the external diameter were between 6 and 11 nm and 11 and 28 nm, respectively, which was beneficial to the dispersion of Pt catalyst, the complete contact between the reactant and catalyst, and the rapid overflow of the hydrogen product.

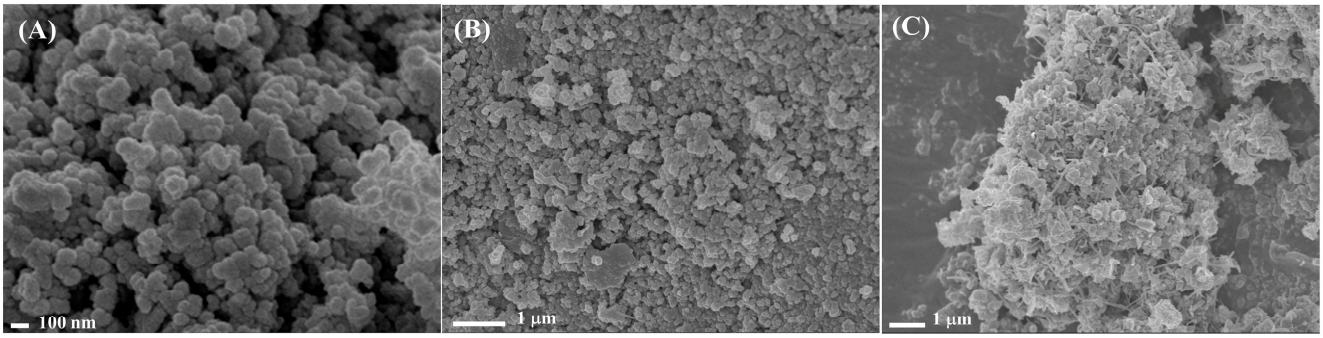

Figure 1. Effect of the solvent on the preparation of CNTs at 800 °C: (**A**) without any solvent, (**B**) H_2O, (**C**) DMSO.

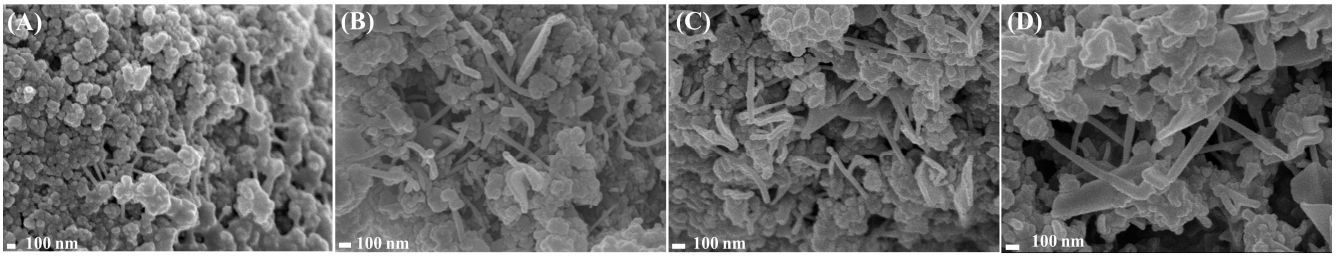

Figure 2. Effect of the temperature on the preparation of CNTs: (**A**) 700 °C, (**B**) 750 °C, (**C**) 800 °C, (**D**) 850 °C.

The specific surface area and pore structure were significant factors for the evaluation of the properties of carbon materials. Compared to C, the structure of the CNTs was significantly changed. As listed in Table 1, the specific surface area of C was high at 64.6 m^2/g, which increased to 138 m^2/g for the CNTs. The same downtrends were observed in the micropore area and pore volume; however, the average pore width decreased from C to CNTs, which may be caused by the formation of tubular structures. The large specific surface area and pore volume could promote the dispersion of Pt atoms to improve the catalytic performance.

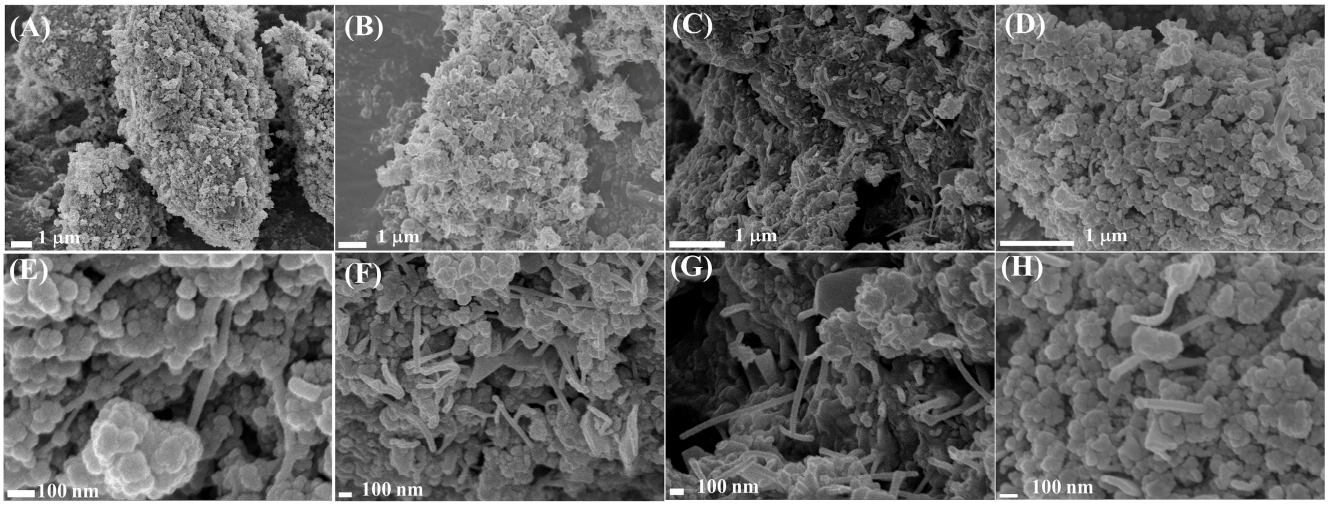

Figure 3. Effect of the time on the preparation of CNTs: (**A**) 4 h, (**B**) 6 h, (**C**) 8 h, and (**D**) 10 h in 1 μm field view and (**E**) 4 h, (**F**) 6 h, (**G**) 8 h, and (**H**) 10 h in 100 nm field view.

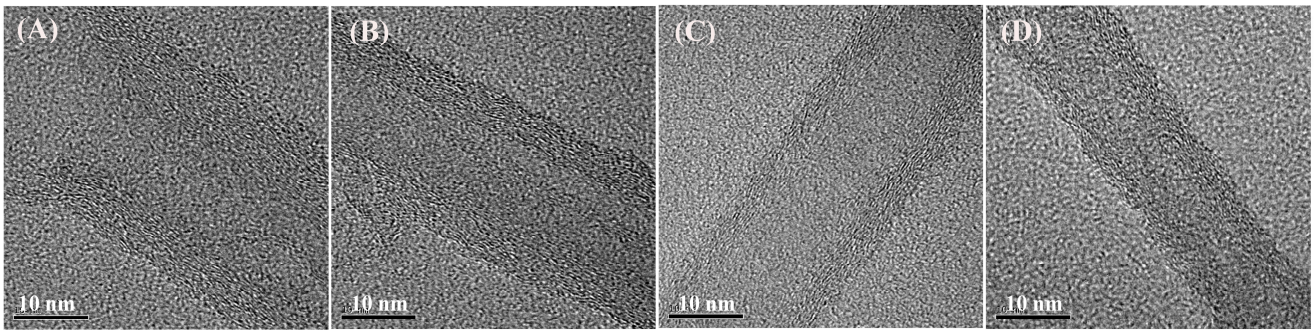

Figure 4. TEM images (**A**–**D**) of the as-prepared CNTs at 800 °C for 6 h in DMSO.

Table 1. Surface structure information of carbon supports.

Supports	BET (m^2/g)	Micropore Area (m^2/g)	Pore Volume (cm^3/g)	Average Pore Width (nm)
C	64.6	12.8	0.282	17.4
CNTs	138	44.9	0.359	10.4

Figure 5 shows the structural characterizations of C and the as-prepared CNTs. As shown in Figure 5A, the diffraction peaks at 24° and 44° in the XRD patterns were derived from the (110) crystal face and (002) crystal face of graphite microcrystalline (PDF# 041-1487), respectively, which evidenced the presence of the crystal structure in the CNTs and C. Compared to C, the two signals of the CNTs were strengthened, which indicated the formation of CNTs. As observed in Figure 5B, the adsorption isotherms of the CNTs and C attached to IV type hysteresis loops, which implied the presence of mesopores. The pore diameter distributions curves suggested that the pore structures of the supports mainly consisted of the mesopores, and the most available apertures were 3~4 nm (Figure 5C), while the pore volume increased from C to the CNTs, manifesting the pore structure was further improved in comparison to that of C. The FTIR spectra (Figure 5D) confirmed that the surface of the CNTs and C possessed abundant and identical oxygen-containing functional groups. The absorption peak at 1630 cm^{-1} was assigned to the stretching vibration of the C=O bond [37]. The region of 3200~3600 cm^{-1} was due to the stretching vibration of the O-H bond [38]. The peak at 1118 cm^{-1} was attributed to the asymmetric stretching vibration of the –O-C=O bond [39]. Raman spectra revealed the graphitization

degree of the carbon materials. As shown in Figure 5E, the peaks at 1353 cm^{-1} (D band) and 1584 cm^{-1} (G band) in the Raman spectrum of the CNTs were attributed to the amorphous carbon (sp^3) and the crystal carbon (sp^2), respectively [40], which were also found in the Raman spectrum of C (i.e., 1341 cm^{-1} and 1591 cm^{-1}). Moreover, the ratio value of I_D/I_G was 0.817 for the CNTs and a little less than that of C (0.943), which indicated that the graphitization degree was improved after C was produced into CNTs [41]. As displayed in Figure 5F, showing the CNTs' TG and DTG profiles, the peak at 106 °C resulted from the loss of moisture, and the peaks at 250 °C and 420~630 °C were ascribed to the decomposition of the carboxyl group and carboxyl anhydrides, respectively [42–44], which was in agreement with the results of the FTIR.

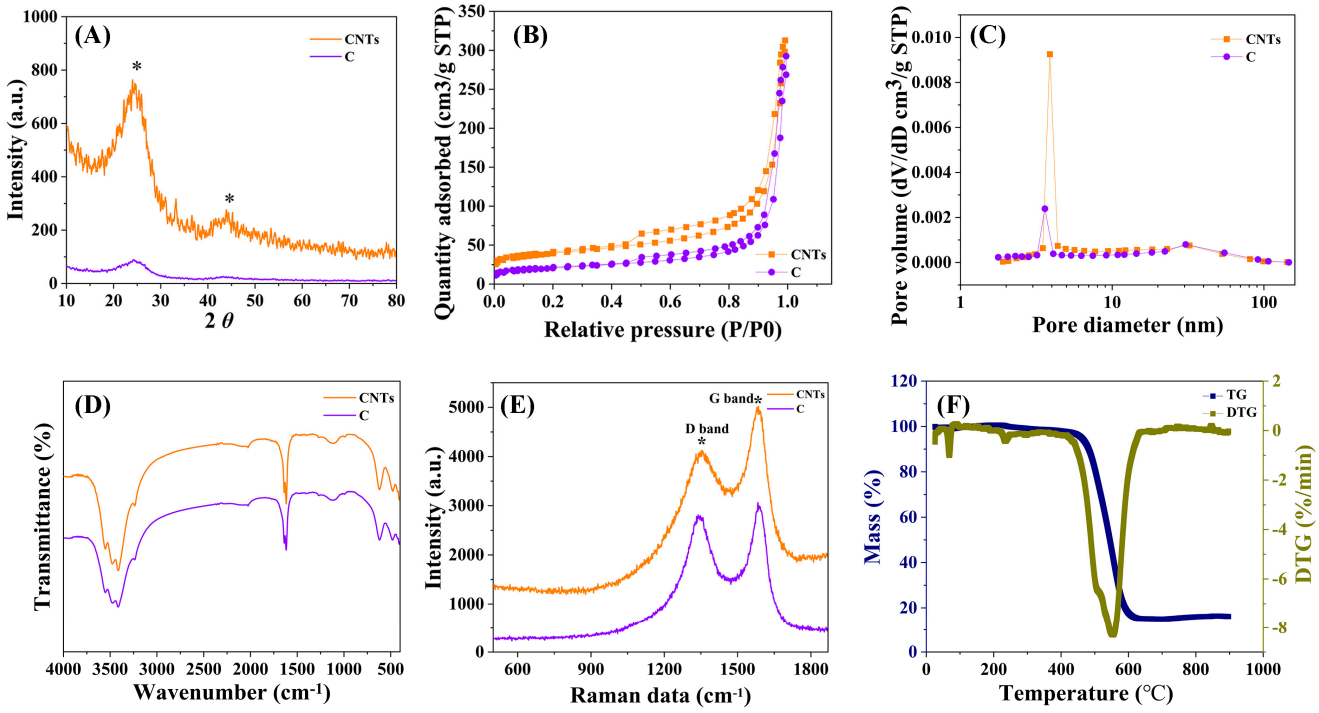

Figure 5. The structural characterizations of CNTs and C. (**A**) XRD, (**B**) N_2 adsorption isotherm, (**C**) pore distribution, (**D**) FTIR, (**E**) Raman spectra, and (**F**) TG profile.

The XPS spectra further verified the surface functional groups of the as-prepared CNTs. The survey spectrum indicated that the surface of CNTs was comprised of C and O elements (Figure 6A). And the C 1s spectrum (Figure 6B) was constituted by the peaks of 284.6, 285.2, and 288.1 eV, which were assigned to the C-C, C-O, and C=O bonds, respectively [45,46]. Meanwhile, the bonds of O-C (531.8 eV) and O=C (533.0 eV) [47] were observed in the O 1 s spectrum of the CNTs (Figure 6C), which was agreement with the results of the FTIR.

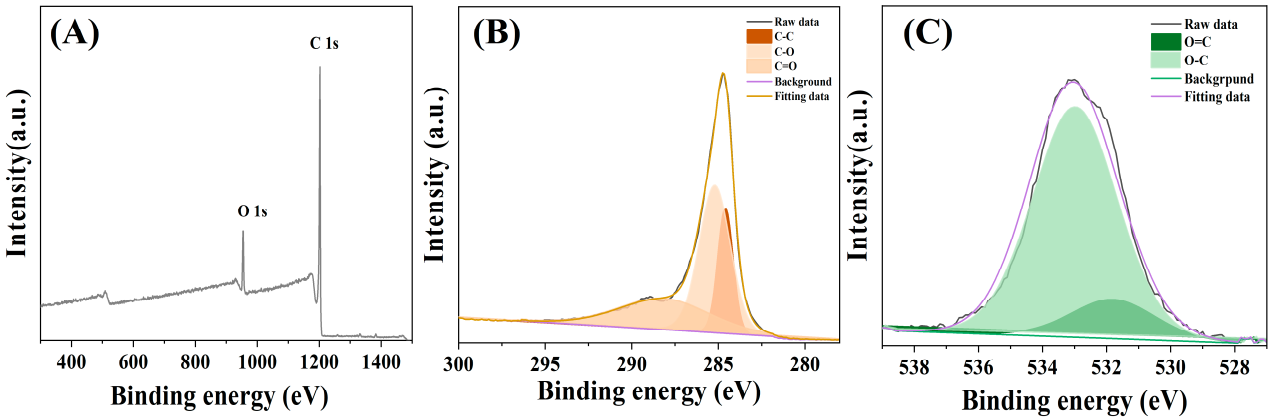

Figure 6. XPS spectra of the as-prepared CNTs: (**A**) survey spectrum, (**B**) C 1 s spectrum, and (**C**) O 1 s spectrum.

3.2. Structure Characterizations of the Pt-Based Catalysts

As shown in Figure S2, the diffraction peaks of Pt were not discovered in the XRD patterns of the Pt/CNTs and Pt/C catalysts, which might result from the low loading amount of Pt or the effective dispersion of the Pt particles on the CNTs and C supports. Figure 7 depicts the TEM images of the Pt/C and Pt/CNTs, which exhibited that the Pt particles appeared well dispersed in the catalysts. The average sizes of the Pt/C and Pt/CNTs catalysts were calculated at about 8.71 nm and 7.01 nm, respectively. The dispersion degrees of the Pt-based catalysts were investigated by the CO pulse adsorption technique, which was listed in Table 2. The dispersion degrees and sizes of the active component Pt were 17.8% and 6.12 nm in the Pt/CNTs catalyst and 12.6% and 8.83 nm in the Pt/C catalyst, which was identical to the result of the TEM images, further indicating the successful preparation of the Pt-based catalysts.

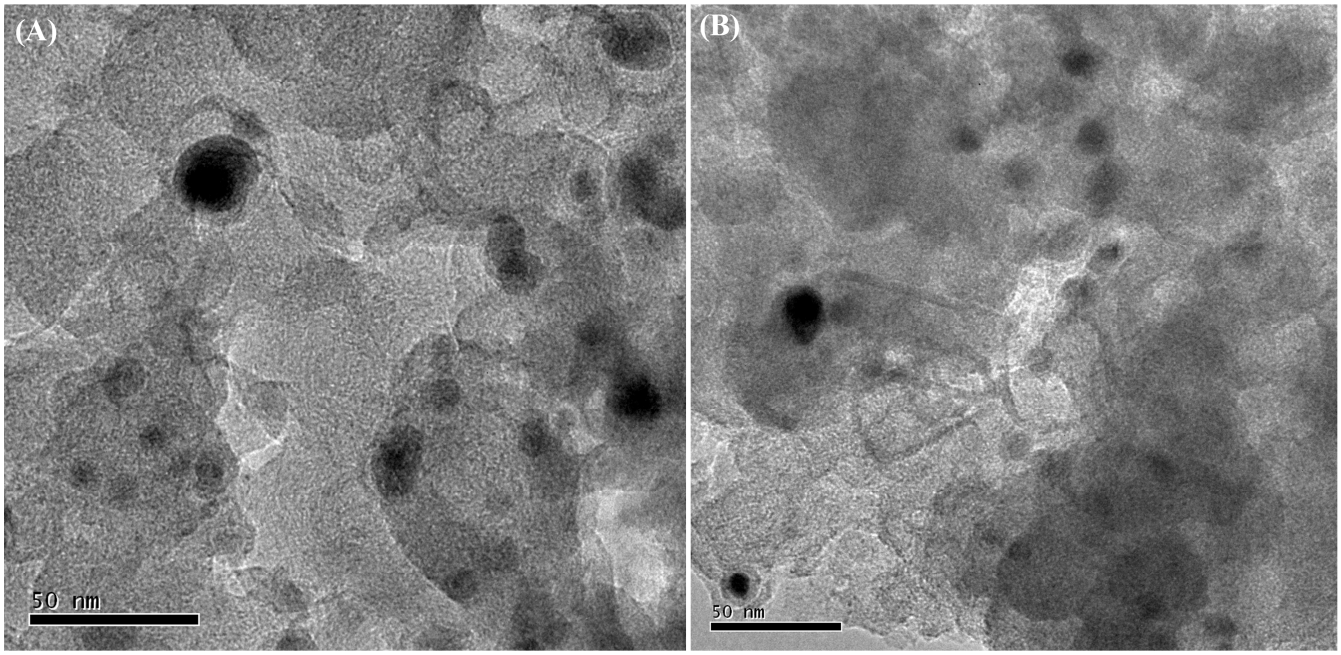

Figure 7. TEM images of (**A**) Pt/C and (**B**) Pt/CNTs.

Table 2. The CO pulse adsorption data of the Pt-based catalysts.

Pt-Based Catalysts	Adsorption Capacity of CO (μL CO/g Catalyst)	Surface Area of Metal (m^2/g Sample)	Dispersion of Active Component (%)	Mean Size of Pt (nm)
Pt/CNTs	41.4	45.2	17.8	6.12
Pt/C	29.5	31.7	12.8	8.83

3.3. Dehydrogenation MCH of the Pt-Based Catalysts

Figure 8 shows the conversion of MCH and the hydrogen evolution using Pt/CNTs, Pt/AC, and Pt/C as catalysts at the reaction temperature of 300 °C and with the space velocity of 5 h^{-1}. As displayed in Figure 8A, the conversion of MCH taking Pt/C as the catalyst was almost zero, which indicated that the carbon black derived from waste tires was not suitable to catalyze the dehydrogenation of MCH. Meanwhile, the conversion of MCH utilizing Pt/AC as the catalyst was 21.2% at 2 h and gradually decreased below 10% at 12 h. Meanwhile, the conversion of MCH applying Pt/CNTs as the catalyst was around 29.6% at 2 h and only slightly decreased to 27.6% at 12 h, which indicated that the Pt/CNTs exhibited much higher and more stable than those of Pt/C and Pt/AC, probably benefiting from the high BET surface and tubular structure to promote the diffusion of MCH, the dispersion of the Pt atoms, and the spilling of hydrogen, as well as the adsorption capacity of hydrogen of CNTs. According to the average conversions of MCH adopting Pt/CNTs (28.6%), Pt/AC (13.6%), and Pt/C (0.19%) as the catalysts, the hydrogen evolution rate of the Pt/CNTs was 336.9 mmol/g_{Pt}/min, much higher than the 160.2 mmol/g_{Pt}/min of the Pt/AC and the 2.23 mmol/g_{Pt}/min of the Pt/C (Figure 8B), further indicating the good performance of the Pt/CNTs in the catalytic dehydrogenation of MCH. Table S1 [16,48–50] lists the comparisons of the hydrogen production reported by the previous literature, which demonstrated the high performance of the resultant CNTs on the hydrogen production at a low Pt load.

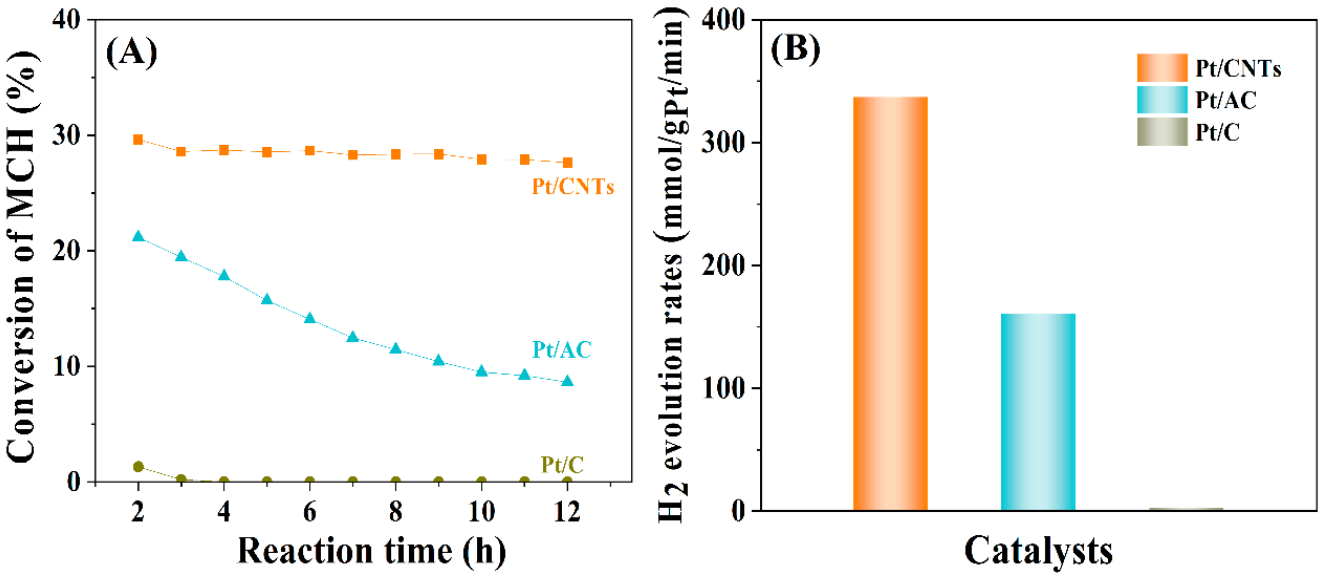

Figure 8. (**A**) The conversion of methylcyclohexane dehydrogenated into toluene and (**B**) the hydrogen evolution based on Pt catalysts.

4. Conclusions

Herein, we proposed a novel utilization of the waste tire pyrolytic carbon for preparing the carbon nanotubes and investigated their application as the support for Pt-based catalysts in the dehydrogenation of methylcyclohexane (MCH) to produce hydrogen. SEM and TEM confirmed the tubular structure and proved the successful production of CNTs. The FTIR, N_2-adsorption, TG profiles, and XPS showed that the yielded CNTs exhibited a large surface

area, abundant pore structure, and oxygen-containing groups. In the dehydrogenation reaction of MCH, the Pt/CNTs catalyst displayed the highest conversion of MCH (28.6%) and the highest hydrogen evolution rate (336.9 mmol/g_{Pt}/min) over those of the Pt/AC (13.6%, 160.2 mmol/g_{Pt}/min) and Pt/C (0.19%, 2.23 mmol/g_{Pt}/min), which was attributed to the tubular structure promoting sufficient contact between the reactants and the catalyst and the rapid leakage of hydrogen. This work provided a new path to deal with waste tires with an eco-friendly and efficient hydrogen storage. Next, we will devote how to improve the yields of the CNTs and further evaluate their application in other fields such as drug delivery, sensors, and electronics.

Supplementary Materials: The following supporting information can be downloaded at: https://www.mdpi.com/article/10.3390/c9040121/s1, Figure S1: SEM of the products prepared by the waste tire pyrolytic carbon in 0.3 mL of H_2O at different times and temperatures; Figure S2: XRD of Pt/C and Pt/CNTs; Table S1: Comparison of the dehydrogenation of MCH over the Pt-based catalysts at 300 °C from the literature.

Author Contributions: Conceptualization, H.Y. and C.Z.; methodology, H.Y.; software, H.Y.; validation, H.Y. and D.H.; formal analysis, C.J. and R.Y.; investigation, H.Y.; resources, S.L.; data curation, C.Z.; writing—original draft preparation, H.Y.; writing—review and editing, C.Z. and S.L.; visualization, S.L.; supervision, S.L.; project administration, C.Z.; funding acquisition, C.Z. All authors have read and agreed to the published version of the manuscript.

Funding: This research was funded by the National Natural Science Foundation of China and the Key Project of Tianjin Application Foundation and Frontier Plan, grant numbers 21003077 and 14JCZDJC32000.

Data Availability Statement: Data are contained within the article and supplementary materials.

Acknowledgments: The authors acknowledge the National Natural Science Foundation of China.

Conflicts of Interest: The authors declare no conflict of interest.

References

1. Nehdi, M.; Khan, A. Cementitious composites containing recycled tire rubber: An overview of engineering properties and potential applications. *Cem. Concr. Aggreg.* **2001**, *23*, 3–10. [CrossRef]
2. Brandsma, S.H.; Brits, M.; Groenewoud, Q.R.; van Velzen, M.J.M.; Leonards, P.E.G.; de Boert, J. Chlorinated Paraffins in Car tires recycled to rubber granulates and playground tiles. *Environ. Sci. Technol.* **2019**, *53*, 7595–7603. [CrossRef] [PubMed]
3. Xu, J.Q.; Yu, J.X.; Xu, J.L.; Sun, C.L.; He, W.Z.; Huang, J.W.; Li, G.M. High-value utilization ofwaste tires: A review with focus on modified carbon black from pyrolysis. *Sci. Total Environ.* **2020**, *742*, 140235. [CrossRef]
4. Bockstal, L.; Berchem, T.; Schmetz, Q.; Richel, A. Devulcanisation and reclaiming of tires and rubber by physical and chemical processes: A review. *J. Clean. Prod.* **2019**, *236*, 117574. [CrossRef]
5. Debnath, B.; Chowdhury, R.; Ghosh, S.K. Sustainability of metal recovery from Ewaste. *Front. Environ. Sci. Eng.* **2018**, *12*, 1–12. [CrossRef]
6. Murillo, R.; Navarro, M.V.; López, J.M.; Garcia, T.; Callen, M.S.; Aylon, E.; Mastral, A.M. Activation of pyrolytic tire char with CO_2: Kinetic study. *Anal. Appl. Pyrolysis.* **2004**, *71*, 945–957. [CrossRef]
7. Darmstadt, H.; Roy, C.; Kaliaguine, S. ESCA characterization of commercial carbon blacks and carbon blacks from vacuum pyrolysis of used tires. *Carbon* **1994**, *32*, 1399–1405. [CrossRef]
8. Lee, W.H.; Kim, J.Y.; Ko, Y.K.; Reucroft, P.J.; Zondlo, J.W. Surface analysis of carbon black waste materials from tire residues. *Appl. Surf. Sci.* **1999**, *141*, 107–113. [CrossRef]
9. Makrigianni, V.; Giannakas, A.; Deligiannakis, Y.; Konstantinou, I. Adsorption of phenol and methylene blue from aqueous solutions by pyrolytic tire char: Equilibrium and kinetic studies. *J. Environ. Chem. Eng.* **2015**, *3*, 574–582. [CrossRef]
10. Salehs, T.A.; Al-Saadi, A.A.; Gupta, V.K. Carbonaceous adsorbent prepared from waste tires: Experimental and computational evaluations of organic dye methyl orange. *J. Mol. Liq.* **2014**, *191*, 85–91. [CrossRef]
11. Han, Y.; Dong, X.T.; Zhang, C.; Liu, S.X. Easy synthesis of honeycomb hierarchical porous carbon and its capacitive performance. *J. Power Sources* **2013**, *227*, 118–122. [CrossRef]
12. Han, Y.; Zhao, P.P.; Dong, X.T.; Zhang, C.; Liu, S.X. Improvement in electrochemical capacitance of activated carbon from scrap tires by nitric acid treatment. *Front. Mater. Sci.* **2014**, *8*, 391–398. [CrossRef]
13. Ji, R.N.; Yu, K.; Lou, L.L.; Zhang, C.; Han, Y.; Pan, S.; Liu, S.X. Chiral Mn (III) salen complexes immobilized directly on pyrolytic waste tire char for asymmetric epoxidation of unfunctionalized olefins. *Inorg. Chem. Commun.* **2012**, *25*, 65–69. [CrossRef]

14. Simaioforidou, A.; Papastergiou, M.; Margellou, A.; Petrakis, D.; Louloudi, M. Activated vs. pyrolytic carbon as support matrix for chemical functionalization: Efficient heterogeneous non-Heme Mn (II) catalysts for alkene oxidation with H_2O_2. *J. Mol. Catal. A Chem.* **2017**, *426*, 516–525. [CrossRef]
15. Seristatidou, E.; Mavrogiorgou, A.; Konstantinou, I.; Louloudi, M.; Deligiannakis, Y. Recycled carbon (RC) materials made functional: An efficient heterogeneous Mn-RC catalyst. *J. Mol. Catal. A Chem.* **2015**, *403*, 84–92. [CrossRef]
16. Zhang, C.; Liang, X.Q.; Liu, S.X. Hydrogen production by catalytic dehydrogenation of methylcyclohexane over Pt catalysts supported on pyrolytic waste tire char. *Int. J. Hydrogen Energy* **2011**, *36*, 8902–8907. [CrossRef]
17. Esfandbod, M.; Merritt, C.R.; Rashti, M.R.; Singh, B.; Boyd, S.E.; Srivastava, P.; Brown, C.L.; Butler, O.M.; Kookana, R.S.; Chen, C. Role of oxygen-containing functional groups in forest fire-generated and pyrolytic chars for immobilization of copper and nickel. *Environ. Pollut.* **2017**, *220*, 946–954. [CrossRef]
18. Zhu, Q.L.; Xu, Q. Liquid organic and inorganic chemical hydrides for high-capacity hydrogen storage. *Energy Environ. Sci.* **2015**, *8*, 478–512.
19. Kariya, N.; Fukuoka, A.; Ichikawa, M. Efficient evolution of hydrogen from liquid cycloalkanes over Pt-containing catalysts supported on active carbons under "wet-dry multiphase conditions". *Appl. Catal. A* **2002**, *233*, 91–102. [CrossRef]
20. Kou, Z.; Zhi, Z.; Xu, G.; An, Y.; He, C. Investigation of the performance and deactivation behavior of Raney-Ni catalyst in continuous dehydrogenation of cyclohexane under multiphase reaction conditions. *Appl. Catal. A* **2013**, *467*, 196–201. [CrossRef]
21. Li, J.F.; Chai, Y.M.; Liu, B.; Wu, Y.L.; Li, X.H.; Tang, Z.; Liu, Y.Q.; Liu, C.G. The catalytic performance of Ni_2P/Al_2O_3 catalyst in comparison with Ni/Al_2O_3 catalyst in dehydrogenation of cyclohexane. *Appl. Catal. A* **2014**, *469*, 434–441. [CrossRef]
22. Zahid, A.H.; Amin, N.; Nisar, F.; Saghir, S. Analysis of MTH-System (Methylcyclohexane-Toluene-Hydrogen-System) for hydrogen production as fuel for power plants. *Int. J. Hydrogen Energy* **2020**, *45*, 32234–32242. [CrossRef]
23. Wijayanta, A.T.; Oda, T.; Purnomo, C.W.; Kashiwagi, T.; Aziz, M. Liquid hydrogen, methylcyclohexane, and ammonia as potential hydrogen storage: Comparison review. *Int. J. Hydrogen Energy* **2019**, *44*, 15026–15044. [CrossRef]
24. Chen, F.T.; Huang, Y.P.; Mi, C.J.; Wu, K.; Wang, W.Y.; Li, W.S.; Yang, Y.Q. Density functional theory study on catalytic dehydrogenation of methylcyclohexane on Pt (111). *Int. J. Hydrogen Energy* **2020**, *45*, 6727–6737. [CrossRef]
25. Yang, X.; Song, Y.; Cao, T.; Wang, L.; Song, H.; Lin, W. The double tuning effect of TiO_2 on Pt catalyzed dehydrogenation of methylcyclohexane. *Mol. Catal.* **2020**, *492*, 110971–110977. [CrossRef]
26. Usman, M.R.; Alotaibi, F.M.; Aslam, R. Dehydrogenation-hydrogenation of methylcyclohexane-toluene system on 1.0 wt % Pt/zeolite beta catalyst. *Prog. React. Kinet. Mech.* **2015**, *40*, 353–366. [CrossRef]
27. Karthikeyan, S.; Pachamuthu, M.P.; Isaacs, M.A.; Kumar, S.; Lee, A.F.; Sekaran, G. Cu and Fe oxides dispersed on SBA-15: A fenton type bimetallic catalyst for N, N-diethyl-p-phenyl diamine degradation. *Appl. Catal. B* **2016**, *199*, 323–330. [CrossRef]
28. Deng, L.; Arakawa, T.; Ohkubo, T.; Miura, H.; Shishido, T.; Hosokawa, S.; Teramura, K.; Tanaka, T. Highly active and stable Pt-Sn/SBA-15 catalyst prepared by direct reduction for ethylbenzene dehydrogenation: Effects of Sn addition. *Ind. Eng. Chem. Res.* **2017**, *56*, 7160–7172. [CrossRef]
29. Osman, A.I.; Abu-Dahrieh, J.K.; Cherkasov, N.; Fernandez-Garcia, J.; Walker, D.; Walton, R.I.; Rooney, D.W.; Rebrov, E. A highly active and synergistic $Pt/Mo_2C/Al_2O_3$ catalyst for water-gas shift reaction. *Mol. Catal.* **2018**, *455*, 38–47. [CrossRef]
30. Obodo, K.O.; Ouma, C.N.M.; Modisha, P.M.; Bessarabov, D. Density functional theory calculation of Ti_3C_2 MXene monolayer as catalytic support for platinum towards the dehydrogenation of methylcyclohexane. *Appl. Surf. Sci.* **2020**, *529*, 147186. [CrossRef]
31. Jiang, Z.; Guo, S.; Fang, T. Enhancing the catalytic activity and selectivity of $PdAu/SiO_2$ bimetallic catalysts for dodecahydro-N-ethylcarbazole dehydrogenation by controlling the particle size and dispersion. *ACS Appl. Energy Mater.* **2019**, *2*, 7233–7243. [CrossRef]
32. Wang, J.; Liu, H.; Fan, S.G.; Li, W.N.; Li, Z.; Yun, H.R.; Xu, X.; Guo, A.J.; Wang, Z.X. Size-dependent catalytic cyclohexane dehydrogenation with platinum nanoparticles on nitrogen-doped carbon. *Energy Fuels* **2020**, *34*, 16542–16551. [CrossRef]
33. Tien, P.D.; Satoh, T.; Miura, M.; Nomura, M. Continuous hydrogen evolution from cyclohexanes over platinum catalysts supported on activated carbon fibers. *Fuel Process Technol.* **2008**, *89*, 415–418. [CrossRef]
34. Kong, H.; Zhou, M.; Lin, G.D.; Zhang, H.B. Pt catalyst supported on multi-walled carbon nanotubes for hydrogenation-dearomatization of toluene and tetralin. *Catal. Lett.* **2010**, *135*, 83–90. [CrossRef]
35. Wang, Y.G.; Shah, N.; Huffman, G.P. Pure hydrogen production by partial dehydrogenation of cyclohexane and methylcyclohexane over nanotube-supported Pt and Pd catalysts. *Energy Fuels* **2004**, *18*, 1429–1433. [CrossRef]
36. Kumar, A.; Kostikov, Y.; Orberger, B.; Nessim, G.D.; Mariotto, G. Natural Laterite as a Catalyst Source for the Growth of Carbon Nanotubes and Nanospheres. *ACS Appl. Nano Mater.* **2018**, *1*, 6046–6054. [CrossRef]
37. Tang, X.D.; Yu, H.M.; Bui, B.; Wang, L.Y.; Xing, C.; Wang, S.Y.; Chen, M.L.; Hu, Z.Z.; Chen, W. Nitrogen-doped fluorescence carbon dots as multi-mechanism detection for iodide and curcumin in biological and food samples. *Bioact. Mater.* **2021**, *6*, 1541–1554. [CrossRef]
38. Pyanova, L.G.; Luzyanina, L.S.; Drozdov, V.A.; Veselovskaya, A.V.; Arbuzov, A.B.; Likholobov, V.A. Study of the effect of a number of oxidizers on variation of composition of surface functional groups, porous structure, and adsorption properties of composite carbon-carbon sorbent. *Prot. Met. Phys. Chem. Surf.* **2010**, *46*, 320–324. [CrossRef]
39. Sandt, C.; Waeytens, J.; Deniset-Besseau, A.; Nielsen-Leroux, C.; Réjassed, A. Use and misuse of FTIR spectroscopy for studying the bio-oxidation of plastics. *Spectrochim. Acta Part A* **2021**, *258*, 119841. [CrossRef]

40. Zhong, Y.L.; Sun, X.T.; Wang, S.Y.; Peng, F.; Bao, F.; Su, Y.Y.; Li, Y.Y.; Lee, S.T.; He, Y. Facile, large-quantity synthesis of stable, tunable-color silicon nanoparticles and their application for long-term cellular imaging. *ACS Nano* **2015**, *9*, 5958–5967. [CrossRef]
41. Zhu, S.; Wang, L.; Li, B.; Song, Y.; Zhao, X.; Zhang, G.; Zhang, S.; Lu, S.; Zhang, J.; Wang, H.; et al. Investigation of photoluminescence mechanism of graphene quantum dots and evaluation of their assembly into polymer dots. *Carbon* **2014**, *77*, 462–472. [CrossRef]
42. Machado, J.; Castanheiro, J.E.; Matos, I.; Ramos, A.M.; Vital, J.; Fonseca, I.M. SBA-15 with sulfonic acid groups as a Green Catalyst for the acetoxylation of α-pinene. *Microporous Mesoporous Mater.* **2012**, *163*, 237–242. [CrossRef]
43. Chen, H.P.; Xie, Y.P.; Chen, W.; Xia, M.W.; Li, K.X.; Chen, Z.Q.; Chen, Y.Q.; Yang, H.P. Investigation on co-pyrolysis of lignocellulosic biomass and amino acids using TG-FTIR and Py-GC/MS. *Energy Convers. Manag.* **2019**, *196*, 320–329. [CrossRef]
44. Viscardia, R.; Barbarossa, V.; Maggi, R.; Pancrazzi, F. Effect of acidic MCM-41 mesoporous silica functionalized with sulfonic acid groups catalyst in conversion of methanol to dimethyl. *Energy Rep.* **2020**, *6*, 49–55. [CrossRef]
45. Ding, H.; Yu, S.B.; Wei, J.S.; Xiong, H.M. Full-color light-emitting carbon dots with a surface-state-controlled luminescence mechanism. *ACS Nano* **2016**, *10*, 484–491. [CrossRef] [PubMed]
46. Ye, H.L.; Shang, Y.; Wang, H.Y.; Ma, Y.L.; He, X.W.; Li, W.Y.; Li, Y.H.; Zhang, Y.K. Determination of Fe(III) ion and cellular bioimaging based on a novel photoluminescent silicon nanoparticles. *Talanta* **2021**, *230*, 122294. [CrossRef]
47. Ma, S.D.; Chen, Y.L.; Feng, J.J.; Liu, J.; Zuo, X.W.; Chen, X.G. One-step synthesis of water-dispersible and biocompatible silicon nanoparticles for selective heparin sensing and cell imaging. *Anal. Chem.* **2016**, *88*, 10474–10481. [CrossRef]
48. Chen, A.; Zhang, W.; Li, X.; Tan, D.; Han, X.; Bao, X. One-pot encapsulation of Pt nanoparticles into the mesochannels of SBA-15 and their catalytic dehydrogenation of methylcyclohexane. *Catal. Lett.* **2007**, *119*, 159–164. [CrossRef]
49. Sugiura, Y.; Nagatsuka, T.; Kubo, K.; Hirano, Y.; Akitoshi, N.; Miyazawa, K.; Iizuka, Y.; Furuta, S. Dehydrogenation of methylcyclohexane over Pt/TiO_2-Al_2O_3 catalysts. *Chem. Lett.* **2017**, *46*, 1601–1604. [CrossRef]
50. Yan, J.; Wang, W.Y.; Miao, L.; Wu, K.; Chen, G.L.; Huang, Y.P.; Yang, Y.Q. Dehydrogenation of methylcyclohexane over Pt-Sn supported on Mg-Al mixed metal oxides derived from layered double hydroxides. *Int. J. Hydrogen Energy* **2017**, *43*, 9343–9352. [CrossRef]